ARTICLES

Journal of Semiconductors
(2022) 43, 032802
doi: 10.1088/1674-4926/43/3/032802

Structural, optical and antimicrobial properties of pure and Ag-doped ZnO nanostructures

Sagar Vikal[1, †], Yogendra K. Gautam[1, †], Anit K. Ambedkar[1], Durvesh Gautam[1], Jyoti Singh[2], Dharmendra Pratap[2, †], Ashwani Kumar[3], Sanjay Kumar[4], Meenal Gupta[5], and Beer Pal Singh[1, †]

[1]Smart Materials and Sensor Laboratory, Department of Physics, Ch. Charan Singh University, Meerut, Uttar Pradesh 250004, India

[2]Department of Genetics and Plant Breeding, Ch. Charan Singh University, Meerut, Uttar Pradesh 250004, India

[3]Nanoscience Laboratory, Institute Instrumentation Centre, IIT Roorkee, Roorkee 247667, India

[4]Department of Physics, University of Rajasthan, Jaipur 302004, India

[5]Department of Physics, SBSR, Sharda University, Greater Noida, Uttar Pradesh, India

Abstract: In the present work, zinc oxide (ZnO) and silver (Ag) doped ZnO nanostructures are synthesized using a hydrothermal method. Structural quality of the products is attested using X-ray diffraction, which confirms the hexagonal wurtzite structure of pure ZnO and Ag-doped ZnO nanostructures. XRD further confirms the crystallite orientation along the *c*-axis, (101) plane. The field emission scanning electron microscope study reveals the change in shape of the synthesized ZnO particles from hexagonal nanoparticles to needle-shaped nanostructures for 3 wt% Ag-doped ZnO. The optical band gaps and lattice strain of nanostructures is increased significantly with the increase of doping concentration of Ag in ZnO nanostructure. The antimicrobial activity of synthesized nanostructures has been evaluated against the gram-positive human pathogenic bacteria, *Staphylococcus aureus* via an agarose gel diffusion test. The maximum value of zone of inhibition (22 mm) is achieved for 3 wt% Ag-doped ZnO nanostructure and it clearly demonstrates the remarkable antibacterial activity.

Key words: zinc oxide; silver; hydrothermal; FESEM; antimicrobial activity; *Staphylococcus*

Citation: S Vikal, Y K Gautam, A K Ambedkar, D Gautam, J Singh, D Pratap, A Kumar, S Kumar, M Gupta, and B P Singh, Structural, optical and antimicrobial properties of pure and Ag-doped ZnO nanostructures[J]. *J. Semicond.*, 2022, 43(3), 032802. https://doi.org/10.1088/1674-4926/43/3/032802

1. Introduction

Nanotechnology is one of the developing fields of research in smart material sciences. It involves efficient manipulation, fabrication and stabilization of matter at an atomic and molecular level that ranges between 1 to 100 nm[1, 2]. Large surface area-to-volume ratio with unique conformation and distribution of nanoparticles (NPs) are responsible for their enhanced physical and chemical properties. The nanomaterials are used for many applications such as catalysis, antimicrobial, agriculture, antioxidant, sensing devices and pharmaceuticals, etc.[3]. Various nanostructured metal–oxide–semiconductors (NMOS) such as zinc oxide (ZnO), copper oxide (CuO), silver oxide (Ag_2O), titanium dioxide (TiO_2), magnesium oxide (MgO) and calcium oxide (CaO) have been studied for their antimicrobial activity. In vitro studies, it has been shown that metal nanoparticles have the ability to prevent several microbial species[4]. In the context of bulk material, NMOS show remarkable antimicrobial properties[5]. Among various NMOS, ZnO is an important inorganic semiconducting material because of its high thermal stability, oxidation resistivity, photo-stability and high electron mobility[6]. ZnO are mostly nontoxic and used for various applications like, photodetectors, UV-LEDs, thin film transistor, solar cells[7] and drug delivery, etc.[8, 9].

ZnO NPs exhibit antibacterial activity against a variety of pathogenic bacteria. The activity includes various process such as the generation of reactive oxygen species (ROS), cell membrane integrity disruption, enzyme inhibition[10]. ZnO NPs also exhibit antibacterial effect by disrupting the integrity of the cell membrane by the loss of phospholipid bilayer integrity and leakage of intracellular components of the cell that leads to cell death[4, 11–15]. Doping is an effective method in order to improve physical and optical properties of ZnO[15].

Among various noble metals, Ag has great potential due to its unique properties such as good oxygen adsorption behavior, relatively non-toxic, cheaper, high thermal conductivity, high solubility, good electrical conductivity etc. Ag-decorated materials are used to treat infections caused by pathogens[16–23]. Ag-doped ZnO nanoparticles have been examined for various biomedical use such as wound and cancer treatment[24–29].

Recently, many researchers have been investigated microstructural effect (nanoparticles, micro/nanoflowers, hybrid nanostructures, hierarchically structures) of Ag-doped ZnO on their antimicrobial performance[30–37]. Bechambi *et al.* also investigated the antibacterial activities using ZnO modified catalysts with various silver contents which they synthesized using a hydrothermal method[38]. Darroudi *et al.* showed the 10 mm inhibition zone by a nickel oxide nanoparticle against the *S. aureus* bacterium prepared by the sol-gel method[39]. Pathak *et al.* observed a significant enhancement in antibacterial activity in prepared Ag-doped ZnO against *S. aureus*. Zone

Correspondence to: S Vikal, sagarvikal97@gmail.com; Y K Gautam, ykg.iitr@gmail.com; D Pratap, pratapbiotech@gmail.com; B P Singh, drbeerpal@gmail.com

Received 30 JULY 2021; Revised 15 NOVEMBER 2021.

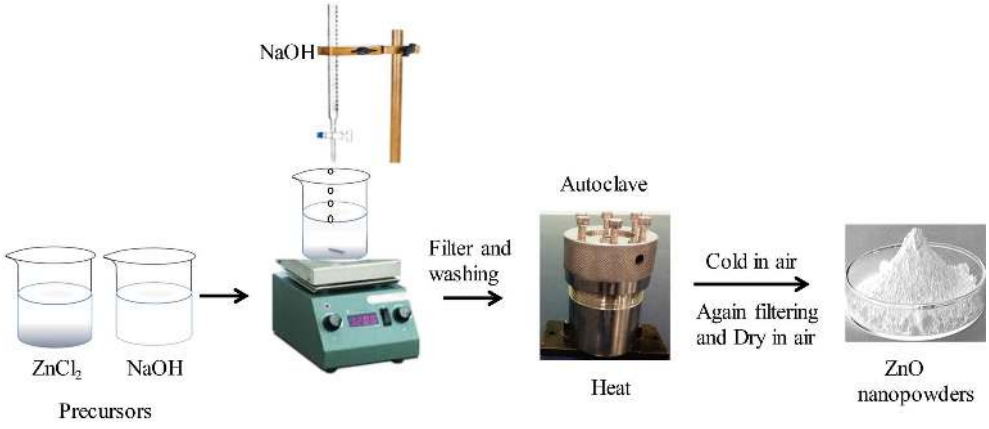

Fig. 1. (Color online) The schematic diagram of hydrothermal method.

of inhibition (ZOI) was recorded 9 and 10 mm against *S. aureus* for pure ZnO and Ag-ZnO NPs, respectively[40]. Ag-ZnO NPs prepared by a green approach using *Cannabis sativa* leaves have shown improved antimicrobial activity (ZOI ~ 16 mm) than the pure ZnO (ZOI ~ 10 mm) [41].

For the synthesis of NMOS, hydrothermal is preferred because it produces high crystalline structures. The hydrothermal method is also cost effective, eco-friendly, easy to handle and known as a low-temperature synthesis method[42].

In this paper, we have been synthesized ZnO nanostructures by using a facile single step hydrothermal method. Antimicrobial properties of pure ZnO and Ag-doped ZnO nanostructures have been investigated.

2. Preparation of nanostructures

ZnO NPs were synthesized by the hydrothermal method using zinc chloride ($ZnCl_2$) (Sigma Aldrich) and sodium hydroxide (NaOH) (Sigma aldrich) as precursors. Different concentration of $ZnCl_2$ and 1 M NaOH solution was prepared in 100 mL distilled water under stirring for 2 h. Furthermore, the ingot solution was retained into the autoclave (Teflon-lined, sealed) and heated at 200 °C for 7 h under autogenously pressure. Thereafter, it was cooled at room temperature. After completion of the process, white precipitate was washed with deionized water and further dried in an oven at 150 °C for 2 h. Finally, the fine powder of pure ZnO NPs was achieved by grinding. Silver nitrate ($AgNO_3$) (Sigma Aldrich) and $ZnCl_2$ were used as precursors to obtain the Ag-doped ZnO nanostructure. $Zn_{1-x}Ag_xO$ (where x = 0.5, 0.75 and 1) fine white powder was obtained via the same process as obtained pure ZnO NPs. ZnO and Ag-doped ZnO nanostructured samples were annealed at 800 °C for 2 h in a muffle furnace. A schematic diagram of hydrothermal process used to synthesis pure and Ag-doped ZnO nanostructures is shown in Fig. 1. The chemical Eqs. (1) and (2) used for synthesizing pure and Ag-doped ZnO nanostructures are as follows:

$$ZnCl_2 + 2AgNO_3 + 4NaOH + H_2O \rightarrow Zn(OH)_2 + 2AgOH + 2NaCl + 2NaNO_3 + H_2O \quad (\text{wash with DD } H_2O \text{ (4 times)}), \tag{1}$$

$$Zn(OH)_2 + 2AgOH \xrightarrow{\Delta} ZnO + Ag_2O + 2H_2O. \tag{2}$$

3. Characterization

The crystal structure, lattice plane and crystallite size of prepared ZnO nanostructures were determined by an X-ray diffractometer (Bruker AXS, D8 Advance). The XRD pattern was recorded by CuK_α radiation with about 1.54060 Å (2θ range from 20° to 80°). The surface morphology of ZnO nanostructures was examined by FESEM (FEI, Quanta 200F) and their composition was determined by energy dispersive X-ray analysis (EDX). Photoluminescence (PL) (FLS 980, Edinburgh Instrument) was used to study the optical properties of the prepared ZnO nanostructures.

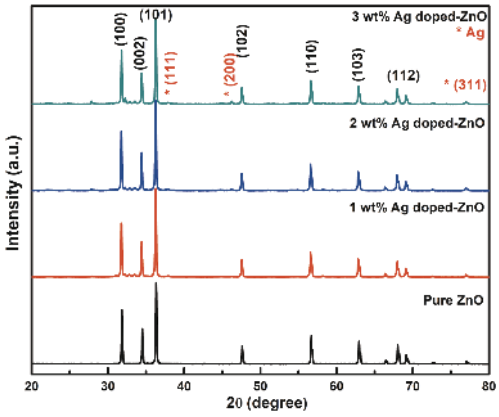

Fig. 2. (Color online) XRD patterns of pure and Ag-doped ZnO nanostructures.

4. Antibacterial activity of ZnO NPs

The agar well diffusion method[43] was used to investigate the antibacterial activity of the prepared ZnO nanostructures against gram positive bacterial strain of *Staphylococcus aureus*. One mL of active secondary culture (1×10^8 CFU) of *S. aureus* was swabbed uniformly onto sterile petri plates containing Luria-Bertani agar media. The plates were punctured using cork borer to make four wells each having diameter of 8 mm. The wells were loaded with 100 μL of distilled water (negative control), Ampicillin (Antibiotic), $ZnCl_2$ (precursor) and ZnO nanostructure further each were incubated at 37 °C for 24 h in dark. The experiment was repeated in triplicate and zones of inhibition observed were recorded and measured.

5. Results and discussion

5.1. Structural study of pure ZnO and Ag-doped ZnO nanostructures

XRD pattern of pure ZnO and Ag-doped ZnO nanostruc-

Table 1. Crystallite size and lattice parameters of pure ZnO and Ag-doped ZnO nanostructures.

S. No.	Sample	Lattice parameters (Å)		Lattice strain (10^{-3})	Crystallite size from XRD (nm)	Band gap (eV)
		$a = b$	c			
1	Pure ZnO	3.24090	5.19128	1.36	50.74	2.35
2	1 wt% Ag-doped ZnO	3.24640	5.20163	1.48	48.34	3.17
3	2 wt % Ag doped ZnO	3.24818	5.20433	1.61	48.20	3.18
4	3 wt% Ag doped ZnO	3.24871	5.20503	1.68	47.32	3.19

tures with different Ag doping concentrations are shown in Fig. 2. The diffraction peaks are observed at 2θ values of 31.76°, 34.41°, 36.24°, 47.62°, 56.54°, 62.88°, 67.93° and 69.09°, for the reflection from lattice planes (100), (002), (101), (110), (103), (112), (201) and (200), respectively and all are good matches with pure ZnO structure [JCPDS card number 36-1451]. The XRD patterns of Ag-doped ZnO nanostructures show the reflections at 38.04°, 44.30° and 77.35° corresponding to Ag along the lattice planes (111), (200) and (311), respectively [JCPDS card number 04-0783]. The crystallite sizes of ZnO nanostructures are observed to be decreased with increase of Ag doping concentration (Table 1). This crystallite size modification could be due to the fact that ionic radii of Ag (0.126 nm) are far greater than that of Zn (0.074nm)[44]. Furthermore, slight peak shifting and the decrease of crystallite size of ZnO in XRD pattern of Ag-doped ZnO (Fig. 2) affirms the incorporation of Ag^+ ions in the ZnO lattice sites. The observed peaks of Ag in the XRD patterns clearly shows the formation of crystalline Ag clusters in the nanostructures as reported in earlier studies[44]. Similar to other monovalent dopant such as Na^+ and K^+, Ag has also occupied both the lattice and interstitial sites[44]. The intensity of the XRD peaks of Ag corresponding to the planes (111), (200) and (220) increases with the increasing doping concentration of Ag in ZnO (Fig. 2). As the Ag concentration increases, the diffraction peaks gradually increase towards the higher angle clearly suggests the successful incorporation of Ag in ZnO[38, 45]. The crystallite orientation is observed along the *c*-axis, (101) plane for all the synthesized pure ZnO and Ag-ZnO-doped nanostructures. This highest intensity of the XRD peaks along (101) plane in pure ZnO is due to the low surface energy with favorable condition for the growth along (101) orientation[18]. While the high intense XRD peak along (101) plane in the Ag-doped ZnO nanostructures is the result of heterogeneous nucleation enabled in the existence of Ag^+ ions. The growth rate in the (101) direction may be enhance by the reduction in doping stress in the ZnO lattice caused by the larger radius of Ag^+ ions than the host Zn^{2+} ions[18].

The crystallite size of pure ZnO and Ag-doped ZnO nanostructures were calculated by Scherrer's formula[18] for high intense peak of plane (101) and the corresponding values are given in Table 1. The crystallite size is found to be reduced from ~ 51 to 47 nm with Ag doping concentration of 0–3 wt%. Lattice constant (*a* and *c*) of prepared ZnO nanostructures were computed by using Eq. (3) [46].

$$\frac{1}{d^2} = \frac{4}{3}\left(\frac{h^2 + hk + k^2}{a^2}\right), \tag{3}$$

where *d* and (*hkl*) are inter-plane spacing and miller indices, respectively. Lattice parameters (*a* and *c*) are defined as:

$$a = \frac{\lambda}{\sqrt{3}\sin\theta}, \quad c = \frac{\lambda}{\sin\theta},$$

where λ and θ are X-ray wavelength and Bragg's angle, respectively. It has been found that lattice parameters of Ag-doped ZnO nanostructures are increased with the increase of Ag doping content in ZnO (Table 1). This is due to the tiny ionic radius of Zn in compare to ionic radius of Ag[47].

Williamson's and Hall's Eq. (4)[46] was used to obtain the lattice strain (ε) of synthesized nanostructures.

$$\beta\cos\theta = \frac{0.9\lambda}{D} + 4\varepsilon\sin\theta, \tag{4}$$

where β, λ, D, θ and ε is full width at half of the maximum (FWHM), wavelength of X-ray used, crystalline size, Bragg's angle, and lattice strain, respectively. The values of lattice strain (ε) are increased due to prompted lattice defects originated by the insertion of Ag in ZnO nanostructures (Table 1). W–H analysis reveals that all ZnO particles have positive (tensile) lattice strain (Fig. 3) and stretched may be the reason of this strain present in the prepared nanostructures[48]. An enhancement in tensile strain is observed in Ag-doped ZnO nanostructures and this may be due to the reduction in number of unit cell per crystallite with increase of Ag dopant percentage in ZnO[48].

5.2. XPS analysis

Core level spectra is illustrated in the Figs. 4(a)–4(c), corresponding to pure Ag 3d and Zn 2p and Ag-doped ZnO nanostructures probed by X-ray photoelectron spectroscopy (XPS). It is clearly realized that the (1–3 wt %) Ag-doped ZnO nanostructure shows three components: Zn, Ag, and O. The features attributed to the Ag peak is slightly weak due to the incorporation of Ag ions in ZnO due to the small scattering cross section. From the Fig. 4(a), the binding energies 367.5 and 373.6 eV are observed for the peaks of Ag $3d_{5/2}$ and Ag $3d_{3/2}$, respectively. It confirms that the Ag is successfully incorporated within the crystal lattice of ZnO. In Fig. 4(b), two peaks are observed at 1021.4 and 1044.5 eV in the high-resolution spectrum and these are attributed to the Zn $2p_{3/2}$ and Zn $2p_{1/2}$, respectively. It approves the Zn^{2+} oxidation state. Furthermore, a peak is found at 531.2 eV correspond to the O 1s and it is related to the surface hydroxyl oxygen, as shown in Fig. 4(c). The surface hydroxyl oxygen can inhibit photo-generated electron–hole recombination. The elemental analysis (XPS) of the Ag-doped ZnO nanostructure reveals the successful inclusion of Ag atoms into ZnO host matrix[49].

5.3. Surface morphology study of pure ZnO and Ag-doped ZnO nanostructures

The prepared ZnO and Ag-doped ZnO nanostructures were investigated using FESEM in order to examine the surface morphology. The surface morphology and elemental com-

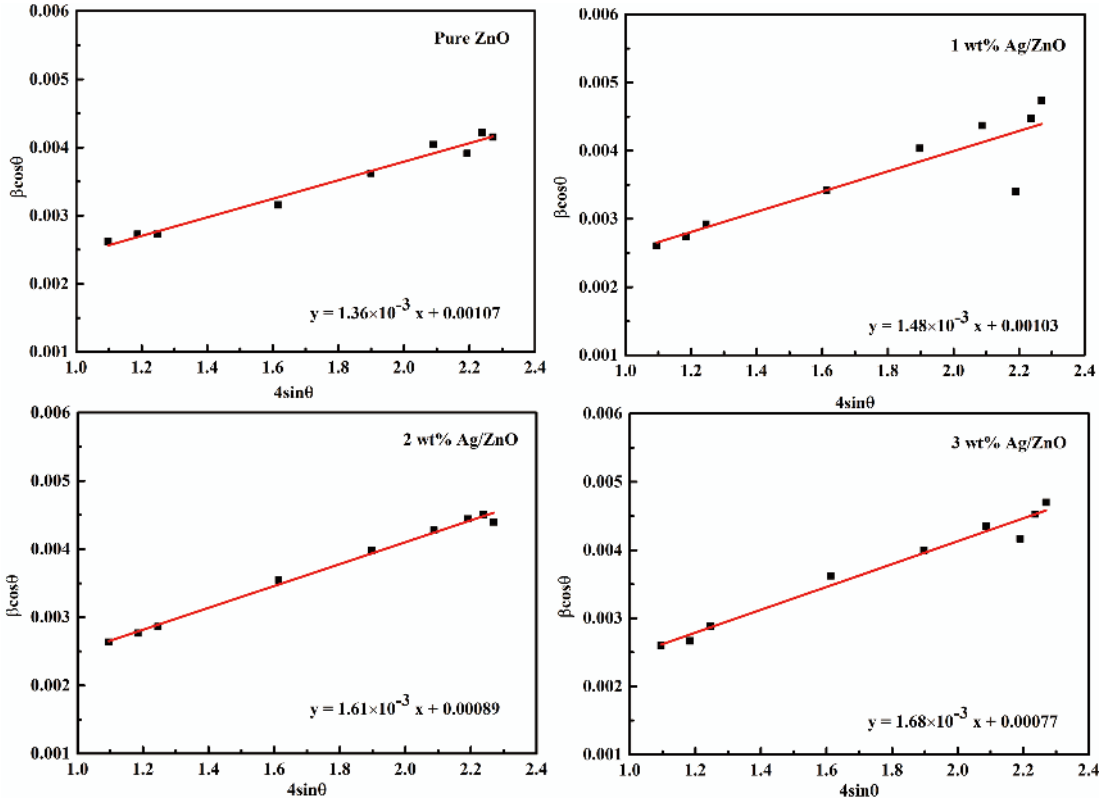

Fig. 3. (Color online) W–H analysis for pure and Ag-doped ZnO nanostructures.

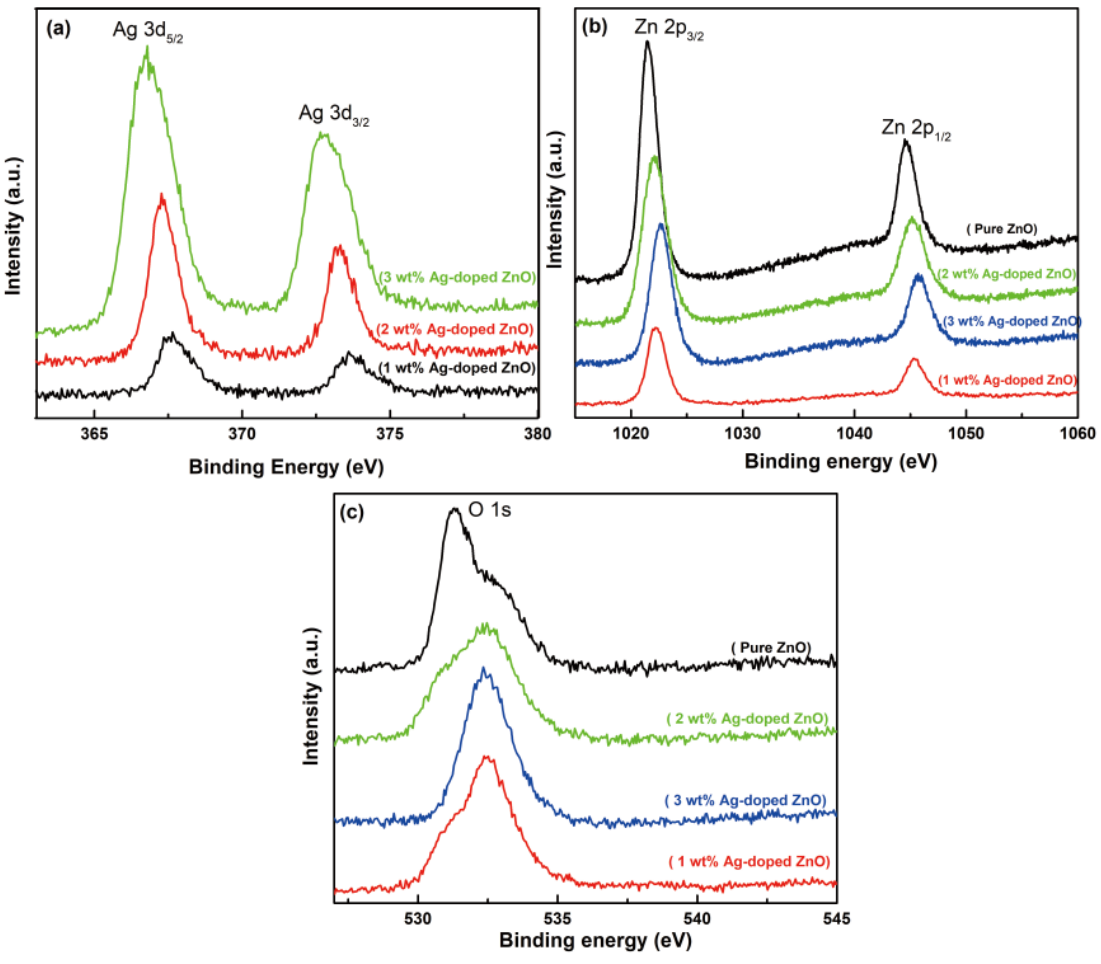

Fig. 4. (Color online) XPS analysis for (a) Ag 3d, (b) Zn 2p and (c) O 1s.

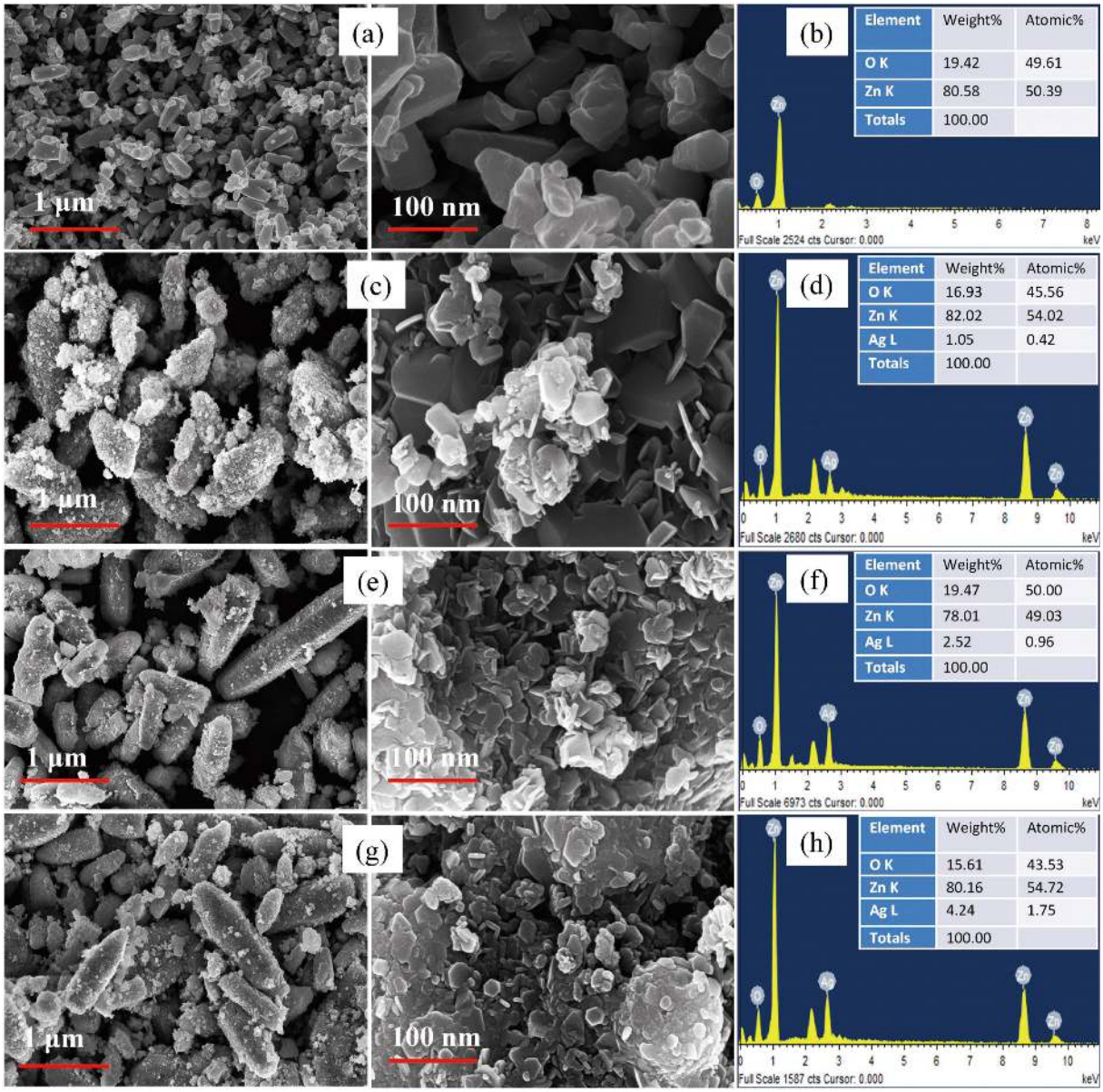

Fig. 5. FESEM with EDAX image of (a, b) pure ZnO, (c, d) 1 wt% Ag-doped ZnO, (e, f) 2 wt% Ag-doped ZnO and (g, h) 3 wt% Ag-doped ZnO.

position of pure ZnO and Ag-doped ZnO nanostructures are shown in Fig. 5. FESEM images of pure ZnO particles demonstrate a hexagonal-like structure. The FESEM results are found to be consistent with XRD results. Ag-doped ZnO nanostructures clearly depicts the needle-shaped nanorods structure with very small diameter [Figs. 5(e) and 5(g)]. The rods have a broad hexagonal base with circular tips. The magnified image shows its hexagonal morphology with pointed tips (Fig. 5(g)). The morphological change from hexagonal (ZnO nanostructures) to needle-shaped nanorods (Ag-doped ZnO nanostructures) could be due to the replacement of Ag^{2+} to Zn^{2+} in the ZnO lattice[44]. The atomic/weight percentage ratio of Ag and Zn presenting in the Ag-doped ZnO nanostructures was estimated by EDX analysis. The elemental analysis (EDAX) confirms that synthesized ZnO and Ag-doped ZnO nanostructures contain Zn, O and Ag elements in their appropriate stoichiometric ratio as shown in Figs. 5(b), 5(d), 5(f), and 5(h).

5.4. Photoluminescence (PL) analysis

The photoluminescence (PL) spectra of pure ZnO and Ag-doped ZnO nanostructures were recorded at room temperature for the wavelength (350–800 nm) (Fig. 6). Xenon lamp with excitation wavelength of 329 nm was used to record PL spectra of all samples. The PL spectra depict two emission bands at wavelength 389 and 527 nm with different intensities for pure ZnO sample. The PL spectra peak analysis reveals

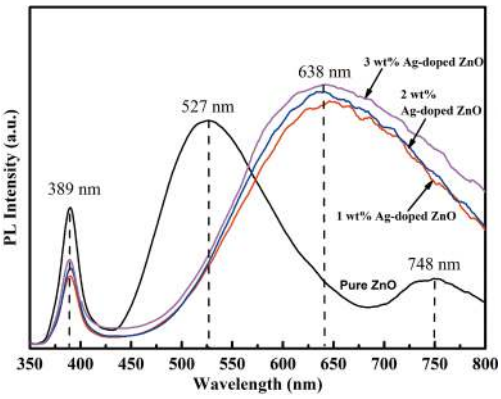

Fig. 6. (Color online) PL emission spectra of pure ZnO and Ag-doped ZnO nanostructures.

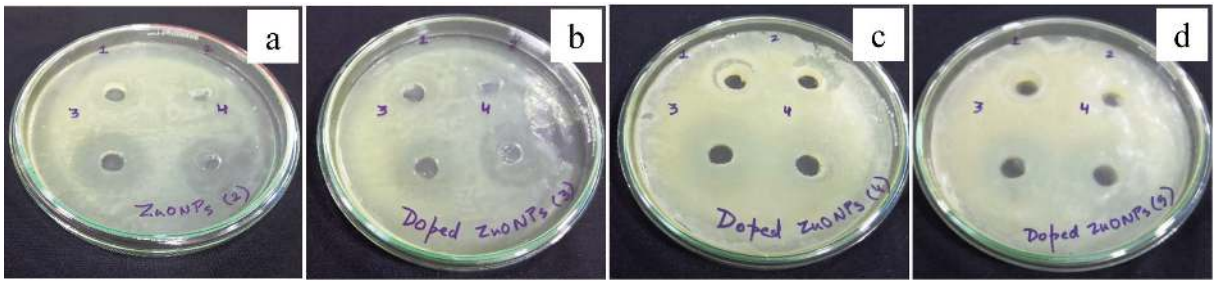

Fig. 7. Zone of inhibition of (a) pure ZnO, (b) 1 wt% Ag-doped ZnO, (c) 2 wt% Ag-doped ZnO, and (d) 3 wt% Ag-doped ZnO.

that peak at 389 nm is ascribed to the optical excitation and broad peak at 527 nm is attributed to oxygen vacancies presenting in ZnO lattice. The peaks at 527 nm for green emission may be due to the radiating defects followed by the interface traps holding on the grain boundaries[50]. The visible emission commonly designated as deep level emission (DLE) might be related to the variation of the intrinsic defects in ZnO such as zinc vacancy, oxygen vacancy, interstitial zinc, interstitial oxygen and antisite oxygen[51].

The green emission is the result of recombination of the electrons in single ionized oxygen vacancies and the recombination of a photo-initiated hole with a single ionized charge state of the point defects (oxygen vacancies and Zn interstitial)[52, 53]. The peak intensity corresponding to 389 nm is related to the oxygen vacancies and it is found to be reduced with an increase in doping concentration of Ag in the ZnO nanostructure.

The intensity at 389 nm initially decreases for 1 wt% Ag doping, and then increases for higher (>1 wt%) Ag doping concentrations. This can be attributed to Ag^+ ions incorporation into the ZnO nanostructures by two different mechanisms: (i) substitution of Zn^{+2} ions fashioning more ionized oxygen vacancies and (ii) including as interstitials Ag. Whereas for low concentration of Ag doping most of the Ag^+ ions might have been inserted into the ZnO lattice substitutionally. In the case of higher Ag doping concentration, the more quantity of Ag^+ ions included into the ZnO nanostructure interstitially. Thus, higher doping concentration of Ag produces more amounts of lattice defects in ZnO nanostructures[44].

While the intensity of the emission peak at 638 nm is decreased with decrease in Ag doping amount (Fig. 6). The presence of Ag nanostructures on the surface of ZnO nanorods may be the cause of this quenching. Further, the peaks at 638 nm for the red emission show a shallow level emission (DLE) associate with the localized levels[54]. Because the defects in pure and Ag-doped ZnO samples, are found doping (Ag) concentration dependent. The energy band gaps of pure ZnO and Ag-doped ZnO nanostructures were calculated by PL spectra using Eq. (5)[55] and the values are listed in Table 1.

$$E = \frac{1240}{\lambda_{nm}}, \tag{5}$$

5.5. Antibacterial activity

The antimicrobial activity of synthesized pure ZnO nanostructures and Ag-doped ZnO NPs were assessed and their antibacterial activities against *S. aureus* were clearly observed in the agar well diffusion method. The difference in the zone of inhibition of pure ZnO NPs and Ag-doped ZnO nanostructures in comparison to the Zn^{+2} and Ag^+ ions (100 μL of 0.7 M of $ZnCl_2$ and $AgNO_3$ solution) were evident and recorded. The zones of inhibition of 18 mm for the pure ZnO nanostructures and 19, 20 and 22 mm for Ag-doped ZnO NPs for concentration of 1, 2 and 3 wt%, respectively are achieved (Figs. 7 and 8 and Table 2). The results also show that *S. aureus* exhibits the resistivity against the ampicillin antibiotic at 25 mg/mL concentration similar to earlier reports[56].

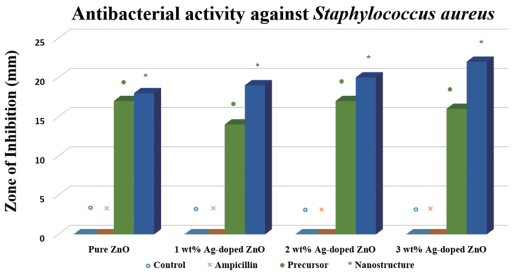

Fig. 8. (Color online) Antibacterial activity of pure ZnO and Ag-doped ZnO nanostructures against Staphylococcus aureus.

Two possible mechanisms have been defined the interaction between bacteria and ZnO nanostructures: (i) decomposition of ZnO results in formation of ROS (hydroxyl radicals, Zn^{2+} ions, singlet oxygen and H_2O_2), which leads to destructive interaction with bacteria and grounds their death and (ii) ZnO nanostructures can gather on the surfaces of bacteria and leads disorganization of cellular function and interruption of cellular membranes. The antibacterial activity of the synthesized ZnO nanostructures might be due to the above defined mechanisms independently or cumulatively[57].

It has been reported that the antibacterial activity of ZnO nanostructures improved with the reducing of particle size. High surface-to-volume ratio of the prepared needle-shaped ZnO NPs is one of the reasons of such enhanced antibacterial activity. Ag doping into ZnO matrix is described to rise the Zn^{2+} ions releasing in water and participating efficiently in the antibacterial activity. An enhancement in Zn ions is probable on the interstitial sites by the doping of Ag ions on the sites of Zn ions in host matrix. These Zn ions may also be easily free from interstitial sites than from their native sites. In addition, Ag^+ ions of Ag-doped ZnO nanostructures may also be released and this leads to the enhancement of the antibacterial activity[58]. Ag doping creates more defects such as Zn interstitial and oxygen vacancies in ZnO host matrix. Hence, Ag doping into ZnO nanostructure enhances efficiently the antibacterial activity due to an increase in the number of Zn^{2+} ions and the defects[58].

6. Conclusions

We have demonstrated the present fast and controlled

Table 2. Zone of inhibition against Staphylococcus aureus bacterium by using pure ZnO and Ag-doped ZnO nanostructures.

S.No.	Types of nanoparticles	Zone of inhibition (mm)			
		Distilled water	Ampicillin	$ZnCl_2$ (precursor)	Nanostructures
1	Pure ZnO	0	0	17	18
2	1 wt% Ag-doped ZnO	0	0	14	19
3	2 wt% Ag-doped ZnO	0	0	17	20
4	3 wt% Ag-doped ZnO	0	0	16	22

one-step method of ZnO nanomaterials preparation by low temperature hydrothermal method. XRD results evaluated the quality of the prepared nanostructures. Ag incorporation in ZnO alters the structural, surface, optical and antibacterial properties. FESEM images depict the change of morphology from hexagonal shape nanostructure (ZnO) to needle-shaped nanorods (Ag-doped ZnO). The synthesized pure ZnO and Ag-doped ZnO nanostructures have shown the antibacterial activity against gram positive human pathogenic bacteria *S. aureus.* A remarkable enhancement in antimicrobial activities is also observed through the doping of Ag in a pure ZnO nanostructure. Hence, the prepared nanostructures possess the profound applications in the pharmaceuticals, cosmeceuticals and agricultural industries.

Acknowledgements

The authors would show their gratitude to Prof. Ramesh Chandra, Institute Instrumentation Centre, Indian Institute of Technology, Roorkee, India for providing FESEM & XRD facilities and Dr. Preetam Singh, NPL, Delhi for his support in PL measurement. The authors would also be grateful to DST, Govt. of India for providing FIST grant for establishing the research facilities in the Department of Physics, Ch. Charan Singh University, Meerut, Uttar Pradesh, India. This work was supported by the UGC, Govt. of India [No. F.30–303/2016(BSR), F.D.Dy. No. 11299]

References

[1] Firdhouse M J, Lalitha P. Biosynthesis of silver nanoparticles and its applications. J Nanotechnol, 2015, 2015, 829526

[2] Song J Y, Kim B S. Rapid biological synthesis of silver nanoparticles using plant leaf extracts. Bioprocess Biosyst Eng, 2008, 32, 79

[3] Moodley J S, Krishna S B N, Pillay K, et al. Green synthesis of silver nanoparticles from Moringa oleifera leaf extracts and its antimicrobial potential. Adv Nat Sci: Nanosci Nanotechnol, 2018, 9, 015011

[4] Seil J T, Webster T J. Antimicrobial applications of nanotechnology: Methods and literature. Int J Nanomedicine, 2012, 7, 2767

[5] Adibkia K. Evaluation and optimization of factors affecting novel diclofenac sodium- eudragit RS100 nanoparticles. Afr J Pharm Pharmacol, 2012, 6, 941

[6] Shi Z F, Zhang Y T, Cai X P, et al. Parametric study on the controllable growth of ZnO nanostructures with tunable dimensions using catalyst-free metal organic chemical vapor deposition. CrystEngComm, 2014, 16, 455

[7] Shi Z F, Xu T T, Wu D, et al. Semi-transparent all-oxide ultraviolet light-emitting diodes based on ZnO/NiO-core/shell nanowires. Nanoscale, 2016, 8, 9997

[8] Bandeira M, Giovanela M, Roesch-Ely M, et al. Green synthesis of zinc oxide nanoparticles: A review of the synthesis methodology and mechanism of formation. Sustain Chem Pharm, 2020, 15, 100223

[9] Firdhouse M J, Lalitha P. Biosynthesis of silver nanoparticles using the extract of *Alternanthera sessilis*-antiproliferative effect against prostate cancer cells. Cancer Nanotechnol, 2013, 4, 137

[10] Cowan M M. Plant products as antimicrobial agents. Clin Microbiol Rev, 1999, 12, 564

[11] Nie L, Gao L, Feng P, et al. Three-dimensional functionalized tetrapod-like ZnO nanostructures for plasmid DNA delivery. Small, 2006, 2, 621

[12] Sharma D, Rajput J, Kaith B S, et al. Synthesis of ZnO nanoparticles and study of their antibacterial and antifungal properties. Thin Solid Films, 2010, 519, 1224

[13] Ahmad M, Ahmed E, Zhang Y W, et al. Preparation of highly efficient Al-doped ZnO photocatalyst by combustion synthesis. Curr Appl Phys, 2013, 13, 697

[14] Kanemitsu Y, Suzuki K, Nakayoshi Y, et al. Quantum size effects and enhancement of the oscillator strength of excitons in chains of silicon atoms. Phys Rev B, 1992, 46, 3916

[15] Salehnezhad L, Heydari A, Fattahi M. Experimental investigation and rheological behaviors of water-based drilling mud contained starch-ZnO nanofluids through response surface methodology. J Mol Liq, 2019, 276, 417

[16] Wu J J, Tseng C H. Photocatalytic properties of nc-Au/ZnO nanorod composites. Appl Catal B, 2006, 66, 51

[17] Avrutin V, Silversmith D J, Morkoç H. Doping asymmetry problem in ZnO: Current status and outlook. Proc IEEE, 2010, 98, 1269

[18] Lupan O, Chow L, Ono L K, et al. Synthesis and characterization of Ag- or Sb-doped ZnO nanorods by a facile hydrothermal route. J Phys Chem C, 2010, 114, 12401

[19] Li X L, He S S, Liu X S, et al. Polymer-assisted freeze-drying synthesis of Ag-doped ZnO nanoparticles with enhanced photocatalytic activity. Ceram Int, 2019, 45, 494

[20] Ansari S A, Khan M M, Ansari M O, et al. Biogenic synthesis, photocatalytic, and photoelectrochemical performance of Ag –ZnO nanocomposite. J Phys Chem C, 2013, 117, 27023

[21] Peng J M, Lin J C, Chen Z Y, et al. Enhanced antimicrobial activities of silver-nanoparticle-decorated reduced graphene nanocomposites against oral pathogens. Mater Sci Eng C, 2017, 71, 10

[22] Takahashi C, Matsubara N, Akachi Y, et al. Visualization of silver-decorated poly (DL-lactide-co-glycolide) nanoparticles and their efficacy against Staphylococcus epidermidis. Mater Sci Eng C, 2017, 72, 143

[23] Shojaie A, Fattahi M, Jorfi S, et al. Hydrothermal synthesis of Fe-TiO_2-Ag nano-sphere for photocatalytic degradation of 4-chlorophenol (4-CP): Investigating the effect of hydrothermal temperature and time as well as calcination temperature. J Environ Chem Eng, 2017, 5, 4564

[24] Dias H B, Bernardi M I B, Marangoni V S, et al. Synthesis, characterization and application of Ag doped ZnO nanoparticles in a composite resin. Mater Sci Eng C, 2019, 96, 391

[25] Khan A U, Yuan Q P, Khan Z U H, et al. An eco-benign synthesis of AgNPs using aqueous extract of Longan fruit peel: Antiproliferative response against human breast cancer cell line MCF-7, antioxid-

ant and photocatalytic deprivation of methylene blue. J Photochem Photobiol B, 2018, 183, 367

[26] Shakeel M, Arif M, Yasin G, et al. Hollow mesoporous architecture: A high performance Bi-functional photoelectrocatalyst for overall water splitting. Electrochim Acta, 2018, 268, 163

[27] Khatami M, Varma R S, Zafarnia N, et al. Applications of green synthesized Ag, ZnO and Ag/ZnO nanoparticles for making clinical antimicrobial wound-healing bandages. Sustain Chem Pharm, 2018, 10, 9

[28] Zhang Y, Mu J. One-pot synthesis, photoluminescence, and photocatalysis of Ag/ZnO composites. J Colloid Interface Sci, 2007, 309, 478

[29] Gouthaman A, Gnanaprakasam A, Sivakumar V M, et al. Enhanced dye removal using polymeric nanocomposite through incorporation of Ag doped ZnO nanoparticles: Synthesis and characterization. J Hazard Mater, 2019, 373, 493

[30] Lam S M, Quek J A, Sin J C. Mechanistic investigation of visible light responsive Ag/ZnO micro/nanoflowers for enhanced photocatalytic performance and antibacterial activity. J Photochem Photobiol A, 2018, 353, 171

[31] Liu Y J, Xu C X, Zhu Z, et al. Self-assembled ZnO/Ag hollow spheres for effective photocatalysis and bacteriostasis. Mater Res Bull, 2018, 98, 64

[32] Zhao J, Wang L, Yan X Q, et al. Structure and photocatalytic activity of Ni-doped ZnO nanorods. Mater Res Bull, 2011, 46, 1207

[33] Andrade G R S, Nascimento C C, Lima Z M, et al. Star-shaped ZnO/Ag hybrid nanostructures for enhanced photocatalysis and antibacterial activity. Appl Surf Sci, 2017, 399, 573

[34] Sharma N, Kumar J, Thakur S, et al. Antibacterial study of silver doped zinc oxide nanoparticles against Staphylococcus aureus and Bacillus subtilis. Drug Invent Today, 2013, 5, 50

[35] Amornpitoksuk P, Suwanboon S, Sangkanu S, et al. Synthesis, characterization, photocatalytic and antibacterial activities of Ag-doped ZnO powders modified with a diblock copolymer. Powder Technol, 2012, 219, 158

[36] Aldalbahi A, Alterary S, Almoghim R A A, et al. Greener synthesis of zinc oxide nanoparticles: Characterization and multifaceted applications. Molecules, 2020, 25, 4198

[37] Karunakaran C, Rajeswari V, Gomathisankar P. Antibacterial and photocatalytic activities of sonochemically prepared ZnO and Ag–ZnO. J Alloys Compd, 2010, 508, 587

[38] Bechambi O, Chalbi M, Najjar W, et al. Photocatalytic activity of ZnO doped with Ag on the degradation of endocrine disrupting under UV irradiation and the investigation of its antibacterial activity. Appl Surf Sci, 2015, 347, 414

[39] Sabouri Z, Akbari A, Hosseini H A, et al. Eco-friendly biosynthesis of nickel oxide nanoparticles mediated by okra plant extract and investigation of their photocatalytic, magnetic, cytotoxicity, and antibacterial properties. J Clust Sci, 2019, 30, 1425

[40] Pathak T K, Kroon R E, Craciun V, et al. Influence of Ag, Au and Pd noble metals doping on structural, optical and antimicrobial properties of zinc oxide and titanium dioxide nanomaterials. Heliyon, 2019, 5, e01333

[41] Chauhan A, Verma R, Kumari S, et al. Photocatalytic dye degradation and antimicrobial activities of pure and Ag-doped ZnO using cannabis sativa leaf extract. Sci Rep, 2020, 10, 7881

[42] Basnet P, Chatterjee S. Structure-directing property and growth mechanism induced by capping agents in nanostructured ZnO during hydrothermal synthesis — A systematic review. Nano Struct Nano Objects, 2020, 22, 100426

[43] Vu X H, Duong T T T, Pham T T H, et al. Synthesis and study of silver nanoparticles for antibacterial activity against Escherichia coli and Staphylococcus aureus. Adv Nat Sci: Nanosci Nanotechnol, 2018, 9, 025019

[44] Zeferino R S, Flores M B, Pal U. Photoluminescence and Raman scattering in Ag-doped ZnO nanoparticles. J Appl Phys, 2011, 109, 014308

[45] Saboor A, Shah S M, Hussain H. Band gap tuning and applications of ZnO nanorods in hybrid solar cell: Ag-doped verses Nd-doped ZnO nanorods. Mater Sci Semicond Process, 2019, 93, 215

[46] Jannane T, Manoua M, Liba A, et al. Sol-gel Aluminum-doped ZnO thin films: Synthesis and characterization. J Mater Environ Sci, 2017, 8 160

[47] Sandeep K M, Bhat S, Dharmaprakash S M. Nonlinear absorption properties of ZnO and Al doped ZnO thin films under continuous and pulsed modes of operations. Opt Laser Technol, 2018, 102, 147

[48] Xu Z Q, Deng H, Li Y, et al. Characteristics of Al-doped c-axis orientation ZnO thin films prepared by the Sol-gel method. Mater Res Bull, 2006, 41, 354

[49] Ai T, Fan Y, Wang H, et al. Microstructure and properties of Ag-doped ZnO grown hydrothermally on a graphene-coated polyethylene terephthalate bilayer flexible substrate. Front Chem, 2021, 9, 661127

[50] Shanthi S I, Poovaragan S, Arularasu M V, et al. Optical, magnetic and photocatalytic activity studies of Li, Mg and Sr doped and undoped zinc oxide nanoparticles. J Nanosci Nanotechnol, 2018, 18, 5441

[51] Anandh B, Shankar Ganesh A, Thangarasu R, et al. Structural, morphological and optical properties of aluminium doped ZnO thin film by dip-coating method. Orient J Chem, 2018, 34, 1619

[52] Yang Y L, Yan H W, Fu Z P, et al. Photoluminescence and Raman studies of electrochemically as-grown and annealed ZnO films. Solid State Commun, 2006, 138, 521

[53] Vanheusden K, Warren W L, Seager C H, et al. Mechanisms behind green photoluminescence in ZnO phosphor powders. J Appl Phys, 1996, 79, 7983

[54] Kaviyarasu K, Geetha N, Kanimozhi K, et al. *In vitro* cytotoxicity effect and antibacterial performance of human lung epithelial cells A549 activity of zinc oxide doped TiO_2 nanocrystals: Investigation of bio-medical application by chemical method. Mater Sci Eng C, 2017, 74, 325

[55] Singh A, Vishwakarma H. Structural, optical, photoluminescence and electroluminescence properties of small ZnO nanocrystals for optoelectronic device applications. Appl Innov Res, 2019, 1, 11

[56] Zou M X, Zhou R R, Wu W J, et al. Antimicrobial resistance and molecular epidemiological characteristics of clinical isolates of Staphylococcus aureus in Changsha area. Chin Med J (Engl), 2012, 125, 2289

[57] Schwartz V B, Thétiot F, Ritz S, et al. Antibacterial surface coatings from zinc oxide nanoparticles embedded in poly(N-isopropylacrylamide) hydrogel surface layers. Adv Funct Mater, 2012, 22, 2376

[58] Jan T, Iqbal J, Ismail M, et al. Synthesis of highly efficient antibacterial agent Ag doped ZnO nanorods: Structural, Raman and optical properties. J Appl Phys, 2014, 115, 154308

Sagar Vikal is working as a Ph.D. Scholar in the Department of Physics, CCS University, Meerut, U.P., India and he has received his M.Phil. (2019) from the same department. He has contributed 3 book chapters in the book titled "Green and Sustainable Nanotechnology" by SPRINGER 2021. His research interest is focused on antimicrobial activity, photocatalytic activity, environmental remedy and gas sensors.

Yogendra K. Gautam is working as Assistant Professor in Department of Physics, CCS University, Meerut, U.P., India. He had also worked as Assistant Professor in Department of Physics, JUET Guna, M. P., India. He has done his Ph.D. in Material Science from IIT Roorkee, India. He has published 35 research papers in reputed journals. He is serving as a reviewer of 10 international journal of repute. His research areas is focused on antimicrobial activity, photocatalytic activity, hydrogen storage, gas sensors and energy storage devices.

Dharmendra Pratap is currently working as Assistant Professor in Department of Genetics & Plant Breeding, CCS University, Meerut, India. He also worked as Assistant Professor in Department of Horticulture, Sikkim Central University, Gangtok. He obtained his Ph.D. from CSIR-NBRI, Lucknow and Post-doctorate from ICGEB, India. He has published more than 20 research papers in reputed journals and currently having H-index 10. His research areas are molecular virology, bio-nanotechnology and okra breeding for developing resistance against biotic stresses.

Beer Pal Singh is working as Professor and Head in Department of Physics, CCS University, Meerut. He has received his Ph.D. (2002) in Physics from C.C.S. University, Meerut, U.P, India. Recently, he had worked as Visiting Professor in Tokyo University of Science, Tokyo, Japan and Visiting Scientist (Raman Fellow) in University of Puerto Rico, Mayaguez, PR, USA for one year. He has published more than 50 research papers in reputed journals. He is serving as a reviewer of several national and international journal of repute. His research interests comprise of thin films, 2D materials, nanostructured materials, metal oxides, semiconducting materials, thin film transistors, sensors and energy storage devices.